Cor Triatriatum Dexter and Right Atrial Mass Causing Severe Inflow Obstruction

Carlos A. Roldan, MD, Carmel Moazez, MD, Jerome Yatskowitz, MD, Daniel Maoz-Metzl, MD, Brian Castlemain, MD, and Edgar Fischer, MD, *Albuquerque, New Mexico*

INTRODUCTION

Cor triatriatum dexter (CTD) accounts for 0.01% to 0.025% of all congenital heart defects in postmortem series.[1] In CTD, a partially opened fibromuscular membrane subdivides the right atrium (RA) into a superior and inferior chamber. If the size of the aperture of the dividing membrane is small, CTD could mimic tricuspid valve (TV) stenosis. However, CTD is commonly incidentally detected, and therefore its clinical manifestations are not well defined.[2,3]

Patients with systemic lupus erythematosus (SLE) with associated antiphospholipid syndrome (APS) are at increased risk of intracardiac inflammatory, thrombotic, infectious, or tumor masses, which can manifest with cardioembolism, intracavitary obstruction, valve regurgitation and/or stenosis, arrhythmias, syncope, or death.[4-8]

The detection of an RA membrane and an RA mass in a patient with SLE and APS may pose not only major morbidity and potential mortality but also diagnostic and therapeutic challenges.

CASE PRESENTATION

A 42-year-old woman was referred for an outpatient transthoracic echocardiogram (TTE) due to complaints of lower extremity edema and dizziness. Medical history included SLE with APS and a presumed thrombotic RA cardiac mass diagnosed at another institution 7 years prior for which warfarin therapy was recommended. However, they were lost to follow-up and clinical and imaging data of the mass were unavailable. The SLE has been well controlled with mycophenolate mofetil 500 mg orally twice a day.

Initial cardiac workup included an electrocardiogram showing normal sinus rhythm, rightward axis and RA abnormality, and a normal chest radiography (Figure 1).

A TTE was performed to evaluate the reported cardiac mass and revealed a large RA mass moving inferiorly into the TV inflow during diastole, causing inflow obstruction as supported by turbulent color-flow Doppler at this level and severely elevated maximum peak and mean gradients of 24 mm Hg and 17 mm Hg, respectively, by color-flow-guided continuous-wave Doppler (Figure 2, Videos 1 and 2). Right atrial dilatation and bowing interatrial septum (IAS) into the left atrium (LA) indicative of elevated RA pressure were noted. The right ventricular (RV) size and function were normal, the estimated RV systolic pressure was 25 to 30 mm Hg, and the left heart appeared normal. Of importance, a membrane-like structure was noted traversing the RA cavity from the lateral wall to the distal IAS suggestive of a CTD (Figure 2).

A pulmonary perfusion scan, which offers higher sensitivity and similarly high specificity to computed tomography (CT) pulmonary angiography for detection of chronic pulmonary thromboembolism with less radiation exposure, was then performed and showed normal perfusion indicative of low probability of associated pulmonary thromboembolism (Figure 3).

To further characterize the RA mass and adjacent structures, a transesophageal echocardiogram (TEE) was performed. Imaging by two-dimensional (2D) biplane TEE demonstrated a large RA mass suggestive of an old thrombus moving inferiorly into the TV inflow during diastole causing obstruction, a membrane dividing the RA into a superior and inferior chamber with an aperture of 1.2 cm, posterior tricuspid annular calcification with a small mass adherent to the atrial side of the annulus suggestive of an acute or subacute thrombus, and RA dilatation with bowing of the IAS toward the LA indicative of high RA pressure (Figure 4, Videos 3 and 4).

In addition, 2D TEE with color-flow Doppler demonstrated the nonobstructive dividing RA membrane with a large (2.0 cm) aperture with nonturbulent flow at this level in contrast to turbulent flow at the TV inflow level caused by the obstructive mass, which was further supported by maximum peak and mean gradients of 19 mm Hg and 14 mm Hg, respectively, by continuous-wave Doppler (Figure 5, Video 5).

Three-dimensional (3D) TEE characterized the large RA mass as elongated, irregularly shaped, multilobed, attached to the anterolateral free wall by a short stalk, and moving superiorly during systole and inferiorly into the TV inflow during diastole (Figure 6, Video 6). Although 3D TEE imaging was mainly aimed at assessing the large RA mass, peripheral portions of the dividing membrane were noted attached circumferentially to the RA walls (Figure 6, Video 6).

The heart team then recommended surgical resection of the RA membrane and masses, especially of the large mass due to its associated severe TV inflow obstruction, risk for pulmonary embolism, and still undefined etiology.

During a right atriotomy, a thickened and calcified membrane with an aperture originating from the RA free wall and extending to the IAS was noted in the middle of the RA, dividing it into 2 chambers. After resection of the membrane, a large, elongated, and calcified mass within the inferior RA cavity attached by a stalk to the anterolateral free wall was resected. The TV leaflets appeared structurally normal with good coaptation. Then a small nodular mass adherent to the

From the Divisions of Cardiology (C..A.R., C.M., J.Y.); Cardiothoracic Surgery (D.M.-M., B.C.); and Pathology, University of New Mexico School of Medicine, Albuquerque, New Mexico (E.F.).

Key Words: Cor triatriatum, Cardiac mass, Tricuspid valve inflow obstruction, Systemic lupus erythematosus, Antiphospholipid syndrome

Correspondence: Carlos A. Roldan, MD, Cardiology Division, University of New Mexico School of Medicine, Albuquerque, NM 87131. (E-mail: *croldan@salud.unm.edu*).

2468-6441

https://doi.org/10.1016/j.case.2024.01.004

VIDEO HIGHLIGHTS

Video 1: Two-dimensional TTE, apical 4-chamber view, demonstrates a large RA mass moving inferiorly into the TV inflow during diastole without adhering to the leaflets but causing TV inflow obstruction. Right atrial dilatation and bowing IAS into the LA indicative of high RA pressure are also noted.

Video 2: Two-dimensional TTE, reversed and right heart–focused apical 4-chamber view with color-flow Doppler, demonstrates nonturbulent flow within the RA cavity, in contrast to diastolic turbulent flow with a convergence zone at the TV inflow level caused by the obstructive RA mass.

Video 3: Two-dimensional TEE, midesophageal 4-chamber biplane view, demonstrates a large RA mass moving inferiorly into the TV inflow during diastole without adhering to normal appearing leaflets but causing inflow obstruction. Posterior tricuspid annular calcification and a membrane with an aperture of 1.2 cm dividing the RA into a superior and inferior chamber are also noted.

Video 4: Two-dimensional TEE, midesophageal 4 chamber (22°) view, demonstrates the large and mobile inferior RA chamber mass, the dividing membrane extending from the lateral wall to the IAS with an aperture of 2.0 cm, and an additional small, mobile, and soft tissue echoreflectant mass attached to the calcified posterior TV annulus.

Video 5: Two-dimensional TEE with color-flow Doppler, midesophageal right heart-oriented (82°) view, demonstrates nonturbulent flow at the membrane's large (2.0 cm) aperture in contrast to turbulent flow at the TV inflow caused by the obstructive RA mass.

Video 6: Three-dimensional TEE, midcavity superior to inferior RA view, demonstrates a large RA mass attached to the anterolateral RA free wall by a short stalk moving superiorly during systole and inferiorly into the TV inflow during diastole. Peripheral portions of the dividing membrane are also noted attached circumferentially to the RA walls.

View the video content online at www.cvcasejournal.com.

calcified posterior-septal TV annulus was resected. The intraoperative TEE showed no membrane, no masses, and only mild tricuspid regurgitation.

The resected large RA mass had a well-defined short stalk and was mainly consistent with an old thrombus adherent in part to the atrial muscle, in contrast to the resected small mass from the TV annulus, which was consistent with an acute or subacute thrombus (Figure 7).

The patient had an uncomplicated postoperative course, was discharged home on warfarin and mycophenolate mofetil, and remains clinically stable 34 months after surgical intervention. The most recent follow-up TTE 28 months after surgery showed no recurrent masses and normal appearing and moving TV leaflets but residual mild stenosis mainly due to tricuspid annular calcification with mean gradients of 3.3 to 3.7 mm Hg, mild regurgitation, and stable RV systolic pressure of 25 to 30 mm Hg.

DISCUSSION

The differential diagnosis of an intracardiac mass in a patient with SLE and APS includes Libman-Sacks vegetations (which are both inflammatory and thrombotic), thrombotic vegetations, and infective vegetations.[4-8] Noninfective and infective vegetations in these patients affect mostly (>95%) the left heart valves and rarely the right heart valves and endocardial walls. Of importance, a Libman-Sacks vegetation attached to an RA wall can mimic a thrombus and both can mimic a cardiac myxoma.[7,8] Primary benign cardiac tumors with myxomas as the most common type (~50% of cases) are mostly located in the LA (60%-90% of cases) and uncommonly (12%-28%) in the RA and are usually attached to either the left or right side of the fossa ovale and rarely to the LA or RA walls.[9] Of clinical interest, cardiac myxomas can present with systemic clinical manifestations that mimic those of SLE.[9,10] Lipomas and papillary fibroelastomas are the second (~20% of cases) and third (~15%) most common primary benign cardiac tumors, which affect mainly the pericardium and left heart valves, respectively, and rarely the RA walls. Papillary fibroelastomas can be associated with positive antiphospholipid antibodies and therefore can mimic SLE or APS with Libman-Sacks or thrombotic vegetations.[11] Rare RA involvement by primary (mainly sarcomas) or secondary (lung, esophageal, renal, or skin) malignant tumors can not only mimic RA thrombus but can also clinically mimic SLE.[9,12]

Although the echocardiographic characteristics of the RA masses in the context of our patient's clinical data were suggestive of a large old thrombus and a small acute or subacute thrombus, overlapping echocardiographic characteristics of thrombi with tumors or vegetations regarding their location, size, appearance, shape, and mobility precluded their definite differentiation. Complementary cardiac imaging with ultrasound-enhancing agents, magnetic resonance imaging, or gated CT with positron emission tomography may have helped to clarify further the etiology of the RA masses.[9,13,14] However, in our patient, there was an indication for surgery and no further diagnostic testing was performed a priori.

Our patient had a nonobstructive and incidentally detected CTD. However, associated chronic nonlaminar flow in the upper and lower chambers caused by the dividing membrane in this patient prone to endocardial inflammation and increased thrombogenesis may have contributed to the formation and propagation of thrombi within the inferior RA chamber and TV annulus. Supportive of this hypothesis, Hussain *et al.*[15] reported a 22-year-old woman with previous inferior myocardial infarction and acute pulmonary embolism with a CTD and atrial septal defect on TTE in whom thrombotic masses were found during surgery on the upper chamber side of the dividing ridge, anterior TV annulus, and anterior TV leaflet. The authors proposed that the thickened and calcified ridge and associated abnormal flow led to thrombus deposition on the RA upper chamber with propagation to the TV annulus and anterior leaflet, paradoxical embolism to the right coronary artery, and pulmonary embolism.

As illustrated in our patient, TTE and especially TEE with 2D and 3D imaging allow accurate characterization of intracardiac masses regarding their size, shape, lobulation, echoreflectance, location, mobility, and relation or attachment to cardiac structures. In addition, color-flow Doppler and pulsed and/or continuous-wave Doppler accurately determine the hemodynamic effect of intracardiac masses including cavitary or inflow obstruction or valve regurgitation and/or stenosis. Therefore, echocardiography plays a major role in consolidating a differential diagnosis, determining the need for surgical intervention, preoperative planning and intraoperative assessment of surgical results, and postoperative follow-up for assessment of

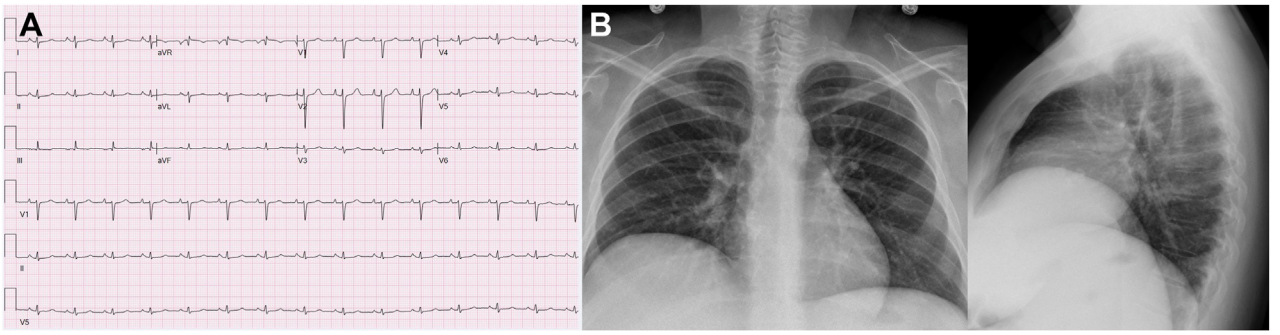

Figure 1 **(A)** Twelve-lead electrocardiogram demonstrates normal sinus rhythm, rightward axis, right atrial abnormality, and poor R-wave progression. **(B)** Anteroposterior and lateral chest radiography demonstrates normal cardiac silhouette with no apparent calcifications, normal great vessels, normal pulmonary parenchyma, and elevated right hemidiaphragm.

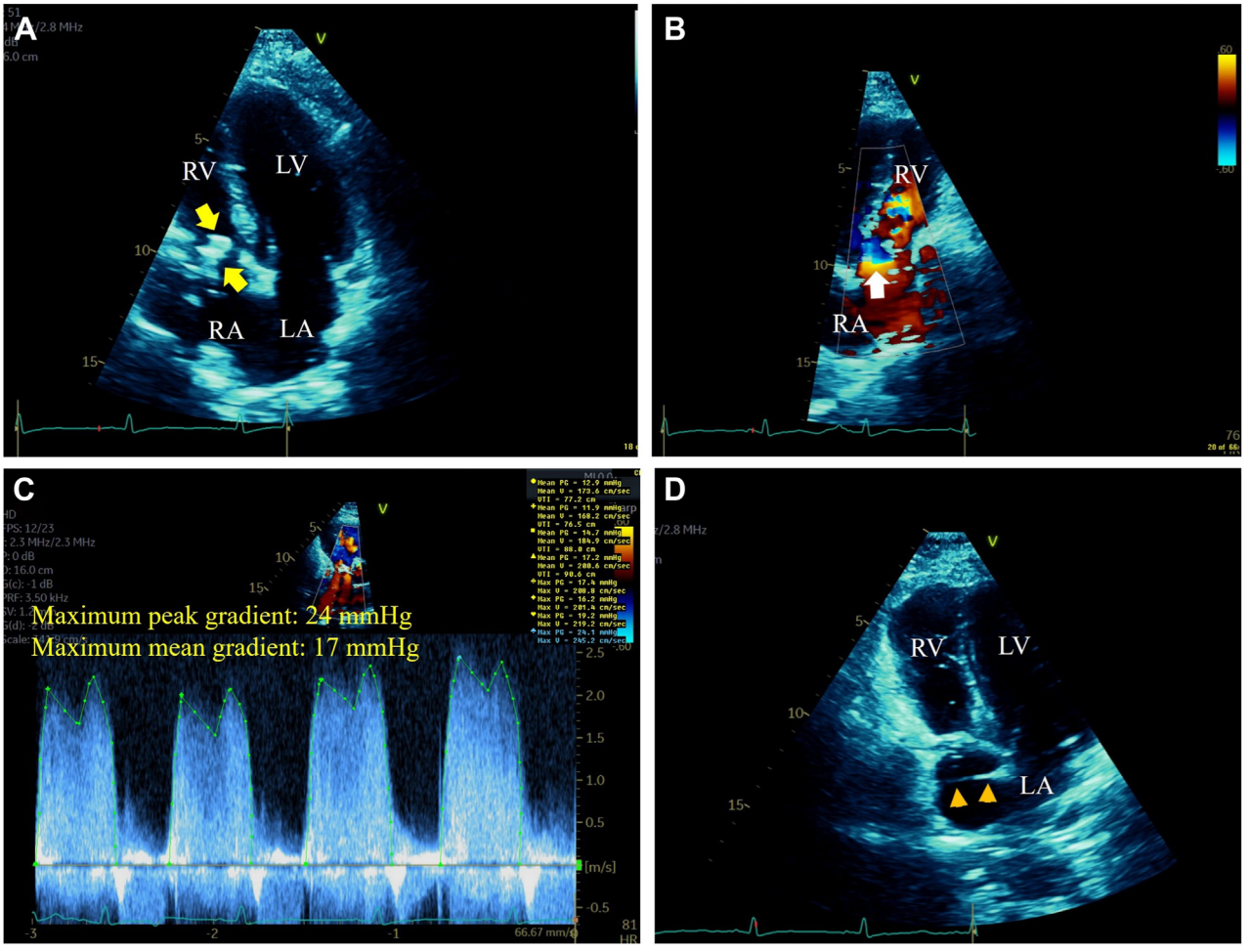

Figure 2 **(A)** Two-dimensional TTE, apical 4-chamber view, during mid-diastole, demonstrates a large (2.5 × 1.5 cm), elongated, irregular, and hyperreflectant RA mass moving inferiorly into the TV inflow (*arrows*). **(B)** Two-dimensional TTE, reversed apical 4-chamber view with color-flow Doppler during late diastole, demonstrates nonturbulent flow within the RA cavity, in contrast to turbulent flow with a convergence zone (*arrow*) at the TV inflow level caused by the obstructive RA mass. **(C)** Two-dimensional TTE, short-axis view, color flow–guided continuous-wave Doppler, demonstrates severe TV inflow obstruction with maximum peak and mean gradients of 24 mm Hg and 17 mm Hg, respectively. **(D)** Two-dimensional TTE, apical 4-chamber view, during early systole, demonstrates a membrane traversing the RA cavity from the lateral wall to the IAS (*arrowheads*) suggestive of a CTD. *LV*, Left ventricle; *RV*, right ventricle.

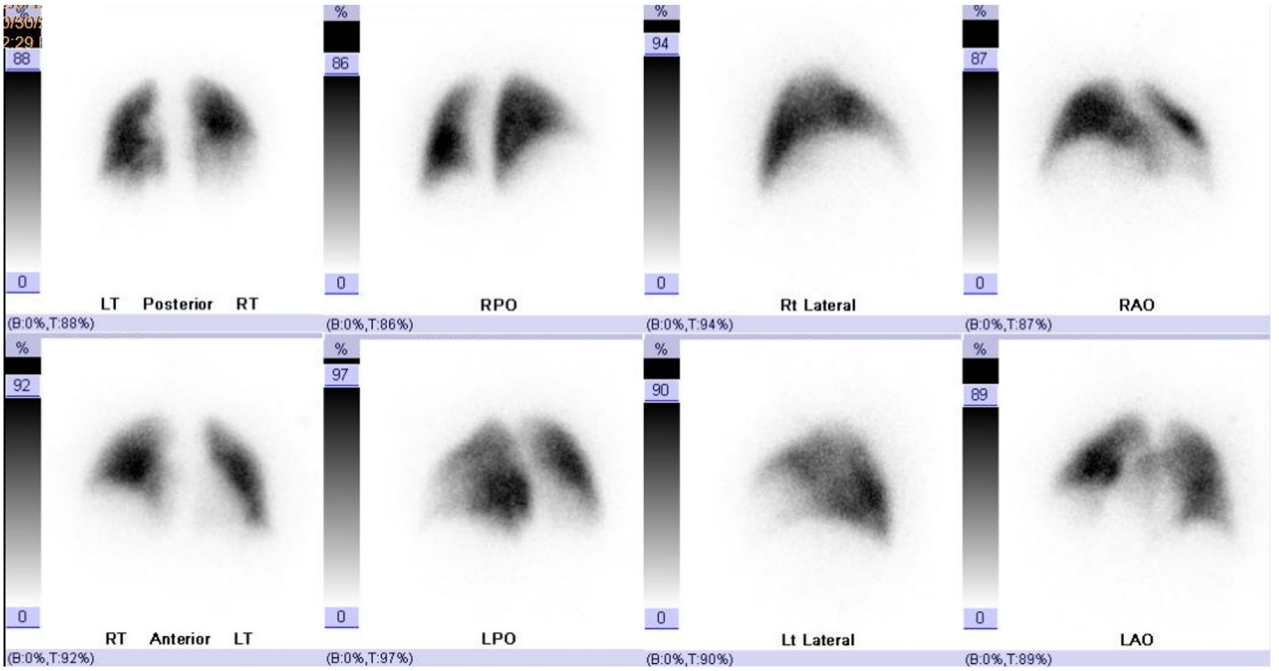

Figure 3 Pulmonary perfusion scan with multiple rotational views demonstrates normal perfusion indicative of low probability of chronic pulmonary thromboembolism.

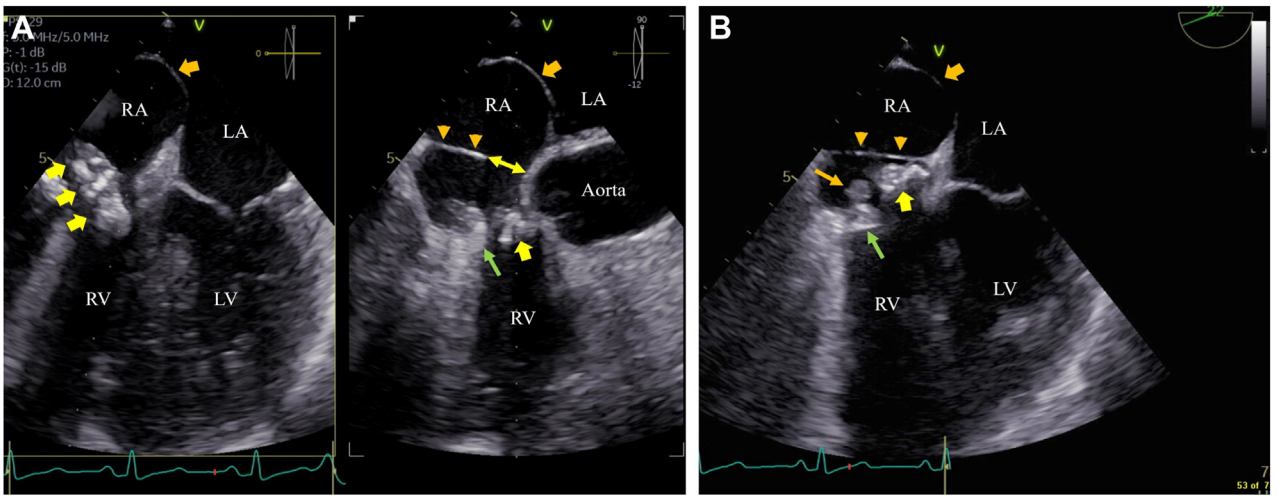

Figure 4 **(A)** Two-dimensional TEE, midesophageal biplane (0°, *left*; 90°, *right*) views during mid-diastole, demonstrates a large (3.3 × 1.5 × 1.1 cm), elongated, and heterogeneously echoreflectant RA mass (*arrows*) moving inferiorly into the TV inflow causing obstruction and a linear, homogeneously echoreflectant, and nonmobile membrane (*arrowheads*) with an aperture of 1.2 cm (*double-headed arrow*) dividing the RA into a superior and inferior chamber. Associated posterior tricuspid annular calcification (*green arrows*) is also noted. In addition, RA dilatation and bowing IAS toward the LA (*orange arrows*) indicative of high RA pressure is noted. **(B)** Two-dimensional TEE, midesophageal 4-chamber (22°) view during midsystole, demonstrates the large RA mass moving superiorly (*arrow*), the dividing atrial membrane extending from the RA lateral wall to the IAS (*arrowheads*), and a small, oval, soft tissue echoreflectant mass (*orange arrow*) adherent to the atrial side of the calcified annulus (*green arrow*). *LV*, Left ventricle; *RV*, right ventricle.

response to any needed pharmacotherapy. However, complementary cardiovascular imaging with magnetic resonance imaging and CT for further tissue characterization are of important diagnostic value. Finally, as in this case, TTE and TEE imaging can also detect, characterize, and define the hemodynamic effects of a CTD.

CONCLUSION

This was a patient with SLE and APS with a nonobstructive CTD, which, compounded by the associated increased inflammation and thrombogenesis of SLE and APS, contributed to the formation and propagation

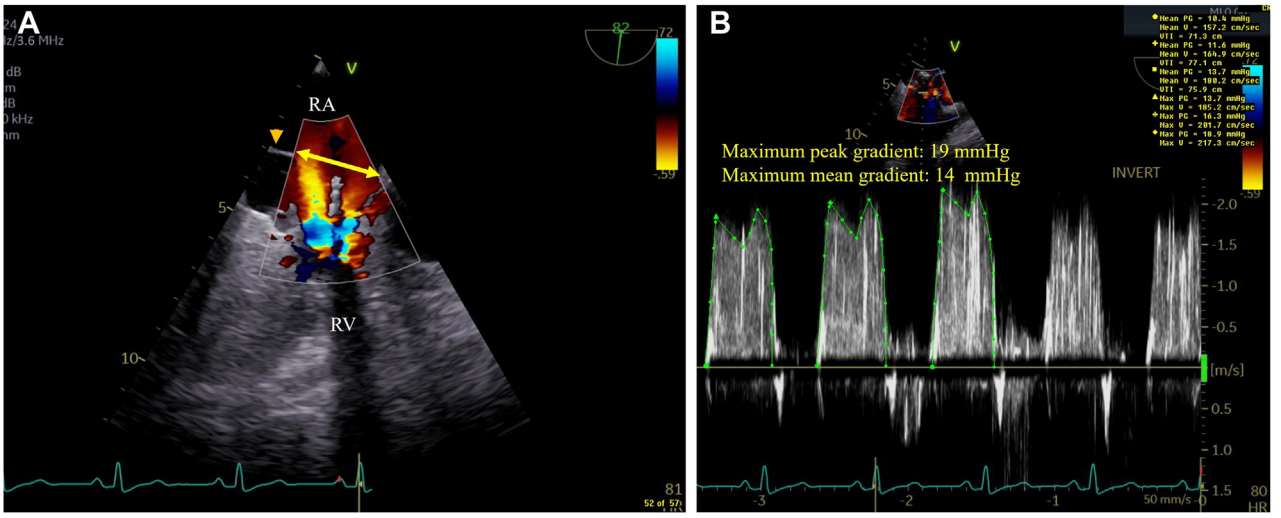

Figure 5 **(A)** Two-dimensional TEE, midesophageal right heart–oriented (82°) view with color-flow Doppler during late diastole, demonstrates the dividing RA membrane (*arrowhead*) with a large (2.0 cm) aperture (*double-headed arrow*) with nonturbulent flow at this level, in contrast to turbulent flow at the TV inflow level (*arrows*) caused by the obstructive mass. **(B)** Two-dimensional TEE, midesophageal right heart–oriented (82°) view with color-flow Doppler-guided continuous-wave Doppler, demonstrates severe TV inflow obstruction with maximum peak and mean gradients of 19 mm Hg and 14 mm Hg, respectively (at a heart rate of 80 bpm). *RV*, Right ventricle.

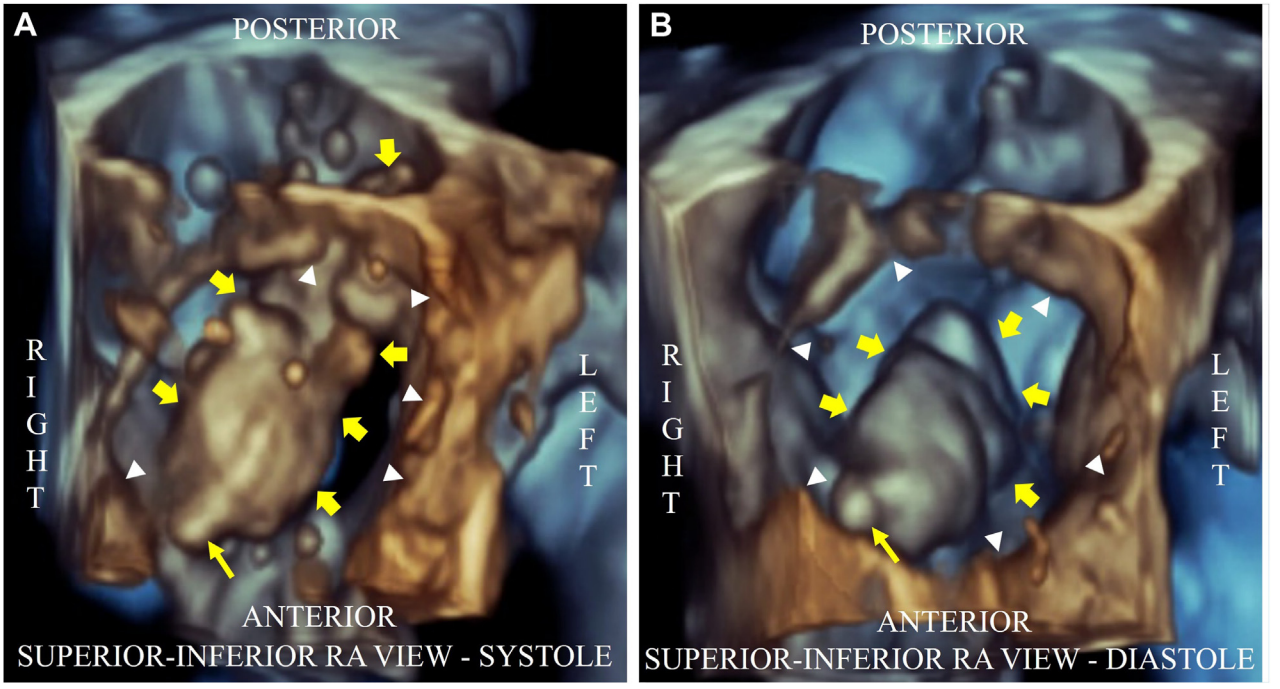

Figure 6 Three-dimensional TEE with a superior to inferior RA view demonstrates the large RA mass (*thick arrows*) attached to the anterolateral free wall by a short stalk (*thin arrow*) moving superiorly during systole **(A)** and inferiorly into the TV inflow during diastole **(B)**. Peripheral portions of the dividing membrane are also noted attached circumferentially to the RA walls (*arrowheads*).

of a large and mainly old thrombus within the inferior RA chamber causing severe and symptomatic TV inflow obstruction. This large RA mass may have also caused traumatic tricuspid annular calcification leading to the deposition of a small acute or subacute thrombus. Finally, meticulous TTE and TEE imaging were key in determining the characteristics, relation to adjacent structures, and hemodynamic impact of CTD and RA and TV annulus thrombi and guiding their successful surgical resection, which ultimately resulted in an excellent clinical outcome.

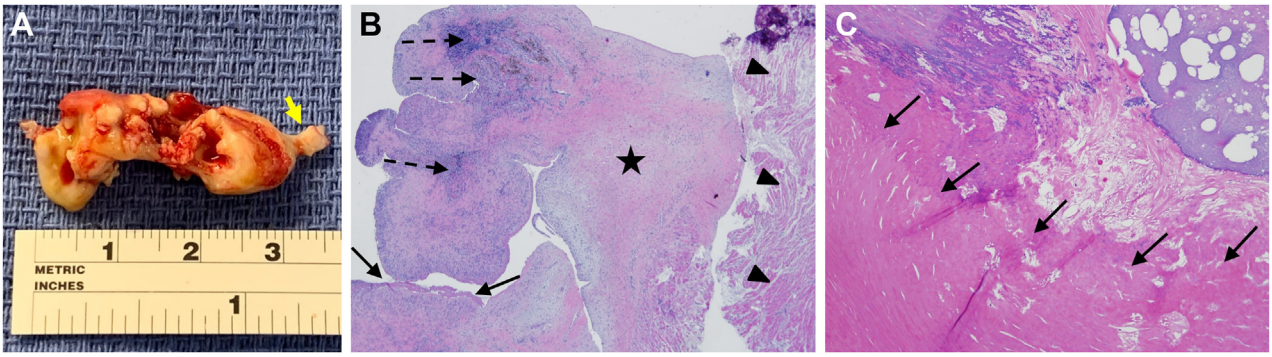

Figure 7 **(A)** Gross pathology demonstrates that the large (3.5 × 1.5 × 1.0 cm) RA mass is elongated, multilobed, irregular, and with a short stalk (*arrow*). **(B)** Histopathology demonstrates a predominantly old thrombus adherent to the atrial muscle (*arrowheads*) with areas of early organization with mild chronic inflammation (*dashed arrows*), areas of denser fibrosis (*star*), and a cap of fresh fibrin thrombus (*arrows*). **(C)** The small mass from the tricuspid annulus demonstrates a layered bright pink eosinophilic acute or subacute thrombus (*arrows*).

ETHICS STATEMENT

The authors declare that the work described has been carried out in accordance with The Code of Ethics of the World Medical Association (Declaration of Helsinki) for experiments involving humans.

CONSENT STATEMENT

The authors declare that since this was a noninterventional, retrospective, observational study utilizing de-identified data, informed consent was not required from the patient under IRB exemption status.

FUNDING STATEMENT

The authors declare that this report did not receive any specific grant from funding agencies in the public, commercial, or not-for-profit sectors.

DISCLOSURE STATEMENT

The authors report no conflict of interest.

SUPPLEMENTARY DATA

Supplementary data related to this article can be found online at https://doi.org/10.1016/j.case.2024.01.004.

REFERENCES

1. Jha AK, Makhija N. Cor triatriatum: a review. Semin Cardiothorac Vasc Anesth 2017;21:178-85.
2. Fuentes Rojas SC, Lawrie G, Faza NN. Cor triatriatum dexter: an innocent bystander. Methodist DeBakey Cardiovasc J 2022;18:10-3.
3. De Michele F, Paparella MT, Forte V, Riccardo D, Chieppa R, Nemore F, et al. Cor triatriatum dexter: a rare incidentaloma. Acta Biomed 2021;93(Supplement 1):e2022093.
4. Roldan CA, Sibbitt WL Jr, Qualls CR, Jung RE, Greene ER, Gasparovic CM, et al. Libman-sacks endocarditis and embolic cerebrovascular disease. JACC: Cardiovascular Imaging 2013;6:973-83.
5. Roldan CA, Tolstrup K, Macias L, Qualls CR, Charlton G, Sibbitt WL. Libman-sacks endocarditis: detection, characterization, and clinical correlates by real time three-dimensional transesophageal echocardiography. J Am Soc Echocardiogr 2015;28:770-9.
6. Chang YS, Chang CC, Chen YH, Chen WS, Chen JH. Risk of infective endocarditis in patients with systemic lupus erythematosus in Taiwan: a nationwide population-based study. Lupus 2017;26:1149-56.
7. Cianciulli T, Saccheri M, Redruello H, Cosarinsky L, Celano L, Trila C, et al. Right atrial thrombus mimicking myxoma with pulmonary embolism in a patient with systemic lupus erythematosus and secondary antiphospholipid syndrome. Tex Heart Inst J 2008;35:454-7.
8. Ozer N, Okutucu S, Karakulak UN, Kes D, Onder S. Libman-Sacks endocarditis mimicking cardiac myxoma. Anadolu Kardiyol Derg 2011;11:E26-7.
9. Tyebally S, Chen D, Bhattacharyya S, Mughrabi A, Hussain Z, Manisty C, et al. Cardiac tumors: JACC CardioOncology state-of-the-art review. J Am Coll Cardiol CardioOnc 2020;2:293-311.
10. Hallward G, Valchanov K. An unexpected pre-operative diagnosis. Eur J Echocardiogr 2010;11:89-90.
11. Roldán-Torres I, Salvador Sanz A, Mora Llabata V, Martí Llinares S, Chirivella González A, Vera Sempere F, et al. Emboligenic mitral papillary fibroelastoma and positive antiphospholipid antibodies. Rev Esp Cardiol 1994;47:255-7.
12. Silva ME, Dábague J, Avila Casado MC, Chévez A, García Torres R, Reyes PA. Does heart sarcoma mimics lupus erythematosus and vasculitis? Report of 2 cases. Arch Inst Cardiol Mex 1999;69:566-9.
13. Mansencal N, Revault-d'Allonnes L, Pelage JP, Farcot JC, Lacombe P, Dubourg O. Usefulness of contrast echocardiography for assessment of intracardiac masses. Archives of Cardiovascular Disease 2009;102:177-83.
14. Wu CM, Bergquist PJ, Srichai MB. Multimodality imaging in the evaluation of intracardiac masses. Curr Treat Options Cardio Med 2019;21:55.
15. Hussain ST, Mawulawde K, Stewart RD, Pettersson GB. Cor triatriatum dexter: a rare cause of myocardial infarction and pulmonary embolism in a young adult. J Thorac Cardiovasc Surg 2015;149:e48-50.